DGLR-2006-146

Nanoparticle reinforced organic-inorganic hybrid coatings for protection of aeronautic structures susceptible to rain and sand erosion

M. Grundwürmer[a, b,*], O. Nuyken[a], M. Meyer[b], J. Wehr[b], N. Schupp[b]

[a]Technische Universität München, Department of Macromolecular Chemistry, Munich, Germany
[b]EADS Corporate Research Centre, Department of Surface and Chemical Engineering, Munich, Germany

Abstract

Erosion protection coatings are developed and characterised in order to protect aeronautic structures susceptible for damage caused by liquid and solid impact e.g. the leading edges of the wings, the radome or the leading edges of rotor blades. Substrates for all coatings are aluminium alloys (AA2024) coated by an epoxy primer. There are two principle sources for erosion damage: sand and rain erosion. This study focuses on the development and characterisation of transparent sol-gel coatings resistant to rain erosion.
The impact of the hardness of the coatings on the erosion protection performance is investigated by varying the ratio of organic-rich to inorganic-rich compounds. Additionally, the mechanical properties of the resulting hybrid coatings are adjusted by nanoparticles (e.g. ZrO_2). Samples are coated by dip-coating. All developed coatings are analysed regarding their adhesion (cross cut), flexibility (impact, mandrel-bending), hardness (nanoindentor) and rain erosion resistance (Stationary Sample Erosion Test). The effect of nanoparticles in sol-gel coatings on the erosion protection behaviour is investigated by light optical microscope.
All sol-gel coatings showed excellent flexibility and adhesion to the substrate. The deformation behaviour of the coatings is visco-elastic. Compared to commercialised erosion protection coatings, particle reinforced hybrid sol-gel coatings increase the resistance against rain erosion. Furthermore, the weight of the protection system is decreased due to the fact that sol-gel coatings reduce the required layer thickness.

Keywords: sol-gel; organic-inorganic hybrid coatings; nanoparticles; liquid impact; rain erosion, aeronautic structures

1. Introduction

Damage caused by solid and liquid impact occurs on leading edges of aeronautic structures such as wing, vertical and horizontal stabilisers, radome, windows as well as on leading edges of helicopter rotor blades. Thus, great efforts are made on the development of protection systems for these parts in the last decades [1-7]. Today erosion protections on planes are uncoated aluminium structures on leading edges or thick rubbery coatings in case of the radome and the stabilisers. For the protection of helicopter rotor blades, different solutions have been investigated in the past. Metals, like aluminium, nickel, titanium or steel play a big role as well as thick adhesive polyurethane tapes. Recent developments focus on thick particle reinforced elastic coatings with a coating thickness up to 1000 µm.
A great number of different types of coatings have been studied with respect to erosion resistance. In general, these coatings can be divided into hard coatings (e.g. SiC, WC, Al_2O_3, DLC) and pliant coatings (PU based organic coatings) [8-9].
This study focuses on the development of new erosion protection systems using a combination of hard and pliant compounds.

2. Erosion by liquid impact

Damage caused by liquid impact was studied in detail in the past [1-8]. This study refers to the failure mechanism by liquid impact as described by J.E. Field et al. A detailed description can be found elsewhere [10]. The theoretical background required for better understanding of this study is given in the following section.
The failure due to liquid impact of a water drop is divided into two regimes. One occurs when the water droplet impacts the surface that may initiate deformation and first cracks in the surface (water

droplet impact). In a second level high velocity lateral water jets can tear away any unevenness in the surface material greater than 100 nm (lateral jets).

Water droplet impact

First damage can occur when the contact edge travels across the surface of the target at a velocity V_c which is greater than the shock wave velocity propagating into the water drop. The water behind the shock front - as a result of the impact - is compressed as there are no free surfaces through which the pressure can be released (Fig. 1). The shock wave velocity into the water drop is reasonably well described, up to impact velocities of 1000 m/s using the following equation:

$$C=C_o+kV \quad (1)$$

where C_o is the acoustic velocity, V is the impact velocity, and k is approximately equal to 2.

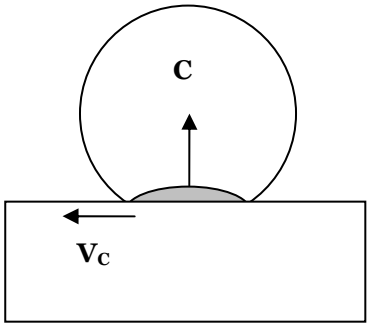

Fig. 1: Droplet after initial impact: water drop is compressed due to lack of free surface [10].

Under the impact conditions considered here, the pressure exerted on the surface of a rigid target is known as the water hammer pressure P_c which is described by the equation:

$$P_c=\rho CV \quad (2)$$

where ρ is the density of the water, 1000 kg/m³.

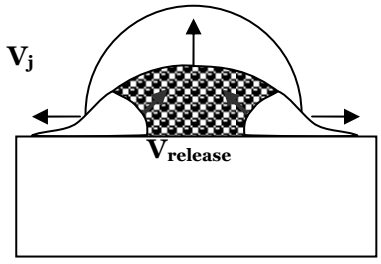

Fig. 2: Droplet after shock wave has over-taken contact edge allowing decompression and jetting [10].

During this phase when the contact edge between target surface and droplet moves faster (V_C) than the shockwave velocity (C) in the droplet water hammer pressures of up to 10^3 MPa may occur. These pressures can cause first cracks in the coating which are the basis for the second stage of the erosion mechanism, the shear stress. [11].

When the shock envelope overtakes the contact edge, a free surface is generated which allows the compressed region to release (Fig. 2).

The release waves propagate into the water drop from the free surfaces, reducing the pressure which is approximately the incompressible Bernoulli pressure P_i:

$$P_i= \rho V^2/2 \quad (4)$$

Liquid impact is conveniently studied in laboratory by extruding a stream of water of known volume through a nozzle or jet. It is possible to relate the damage caused by a particular jet size to that produced by an 'equivalent' spherical drop. The point at which circumferential damage becomes visible at a particular velocity is known as the damage threshold velocity (DTV) [10].

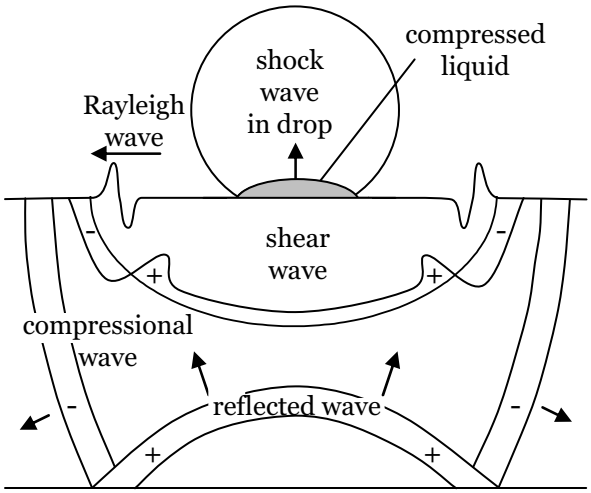

Fig. 3: Impact of a liquid drop impinging the surface of a brittle rigid material. Three types of stress waves are generated in isotropic brittle solids: A compressional wave, a shear wave, and a Rayleigh surface wave [12].

There are three stress waves associated with the target when impacted (Fig. 3). There are two bulk waves (compression and shear) and one surface wave (Rayleigh). The compression wave is the fastest one, whereas the shear wave is slower. The compression wave has little effect on the damage pattern. The third wave is the Rayleigh surface wave which interacts with surface cracks. The Rayleigh wave has both vertical and horizontal components and the depth to which the Rayleigh wave penetrates depends on the wavelength which, in turn, depends on the impact velocity and the drop radius. The impact energy is divided into Rayleigh surface wave with 67.4 % of the total energy of the impact, the shear wave with 25.8 % of the total energy, and the compression wave with 6.9 % of the total energy in case of brittle materials [10].

If an elastic wave reaches a free surface or an interface between solids having different physical properties, the resultant wave reflection and transmission can be of significance in terms of material failure [13]. Spalling and lateral delamination between two coatings can be expected in case that the physical properties of both materials do not match.

Lateral jets

After the first degree of damage (water droplet impact), lateral jets are produced in a second step causing shear stress (Fig. 4). The contact edge between the target surface slows down and is overtaken by the shockfront. Thus, water trapped in the compressed region can escape which generates water jets across the surface causing a high velocity sideways jet of fluid [11]. This fluid has a velocity V_j which is faster than the impact velocity V. Lateral jetting exploits surface asperities which arise from surface roughness or damage, introduced by the Rayleigh surface wave, resulting in material loss and further extension of cracks [10].

Fig. 4: Damage effects of lateral jetting; left hand side damaged by Rayleigh wave only; as lateral jetting crosses surface it tears off asperities it collides with [10].

A great number of test methods are used for the simulation of damage caused by liquid and solid impact [14]. These methods can be divided into Accelerated Sample Erosion Tests (ASET) and Stationary Sample Erosion Tests (SSET). ASET systems realise the required velocity of the droplet impact by acceleration of the sample that impacts on an artificial generated rain field [4, 8]. In case of SSET methods, high velocity water droplets [14] (or single water jets [4, 10, 15, 16]) are impinging on a stationary sample.

3. Conceptual Formulation

As already stated in section 1 two different types of coatings were developed for the purpose of erosion protection in the past: hard inorganic coatings such as SiC, DLC, WC, or Al_2O_3 and pliant, rubbery like organic coatings [8,9]. A technique suitable for the purpose of combining hard and pliant compounds in one coating is the sol-gel process which enables the formation of a highly cross linked network containing organic groups and inorganic parts. The hardness and the flexibility of the coating can be adjusted by the amount of inorganic-rich compounds (Aluminium-sec-butoxide, Zirconium-(IV)-propoxide) as well as by the degree of cross linkage using non-cross linking organic groups (e.g. Alkyl, Phenyl) for increased flexibility and functional groups for the formation of a dense network. The organic-inorganic hybrid network provides sufficient mechanical stability to avoid cracks caused by the rain droplet impact and is flexible enough to absorb the kinetic energy of droplets and sand particles. In addition, the hardness and mechanical resistance of the coatings can be increased by nanoparticle reinforcement. Ceramic oxide and non-oxide particles (e.g. SiC, Si_3N_4, Al_2O_3, ZrO_2, TiO_2, SiO_2) in the range between 10 and 50 nm are uniformly distributed in the coating matrix. Good adhesion of the coating to the substrate can be ensured using precursors containing functional groups which are able to form chemical bonds to the substrate (e.g. epoxy, vinyl, methacrylate). Compared to state of the art erosion protection coatings of 80 - 300 µm the layer thickness is reduced to ~10 µm using the sol-gel technology. An additional advantage of this wet chemical coating process is the transparency which allows the adjustment of the colour of the coating by the basecoat underneath.

A common way to synthesise silica gels is to hydrolyse monomeric, tetrafunctional alkoxide precursors employing a mineral acid (e.g. HCl) or base (e.g. NH_3) as catalyst. Three reactions are generally used to describe the sol-gel process:

(1) Hydrolysis

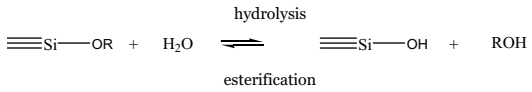

(2) Condensation

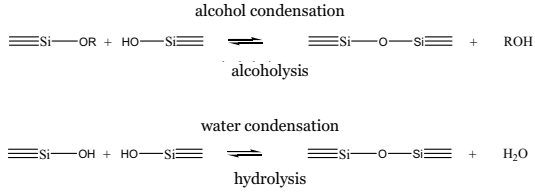

R stands for an alkyl group (C_xH_{2x+1}).

During hydrolysis reactions (1), alkoxide groups (OR) are replaced by hydroxyl groups (OH). Subsequently, condensation reactions (2) take place where silanol groups produce siloxane bonds (Si–O–Si) plus the by-products alcohol (ROH, alcohol condensation) or water (H_2O, water condensation). Under most conditions, condensation starts before hydrolysis is completed [17].

Fig. 5 is a schematic drawing of the compounds of a sol-gel derived erosion protection coating. The metal alkoxide network is based on silica (M_1, Si-O-Si). The hardness of the network can be increased by the use of transition metals (e.g. Ti, V, Zr) and Group III metals (e.g. Al, B) which exhibit,

compared to silicates, greater chemical reactivity resulting from a lower electronegativity of the metal (M_2). Hydrolysis and condensation of these materials lead to the formation of hard nanopareticles embedded into the coating network. In addition, a common way to enhance the hardness of the coating is reinforcement by hard particles (np). It is promising to use particles in the range of a few nanometres to achieve a homogeneous dispersion of these particles within the sol-gel derived particles. Furthermore, the degree of cross-linking is also responsible for the hardness and the mechanical stability of the coatings which is important to avoid first cracks in the layer and crack growth due to a high velocity particle or droplet impact. The required mechanical stability of the network is adjusted by the use of organofunctional alkoxysilanes. Their functional groups (R_1, R_2) are able to form an organic network in addition to the inorganic one [18]. Furthermore, alkoxysilanes with a non-cross-linking group (S; e.g. Phenyl, Alkyl) increase the flexibility as an organic spacer.
Erosion protection coatings have to adhere to the substrate as good as possible. Depending on the substrate the adhesion can be improved by the formation of covalent bonds to the substrate via a condensation reaction of a hydroxyl group or via the organofunctional groups (R_1, R_2).

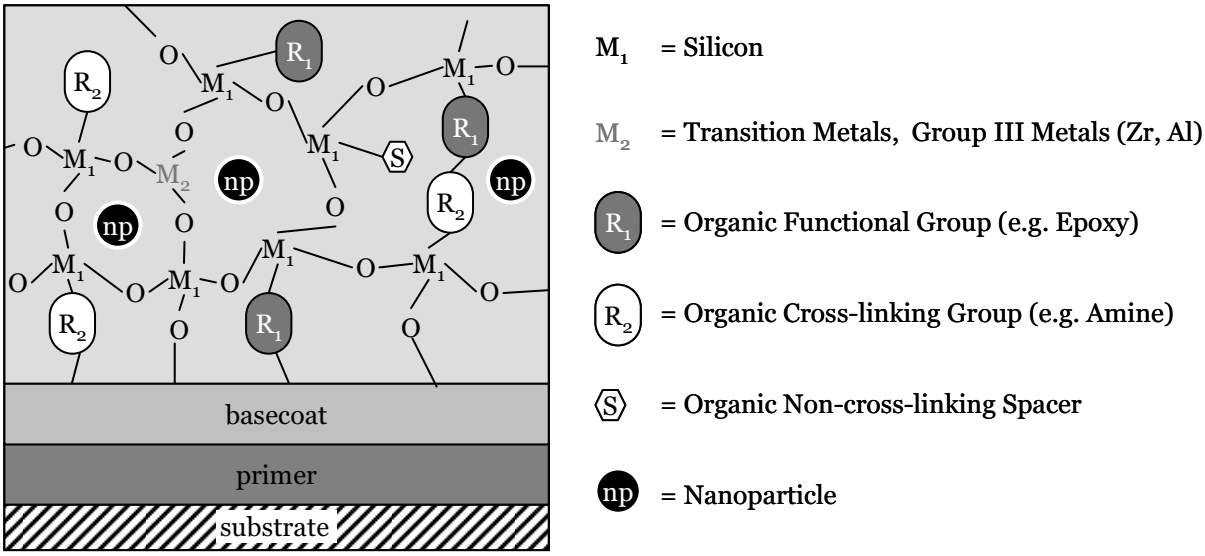

Fig. 5: Schematic layer composition of the organic-inorganic hybrid coating reinforced by nanoparticles based on silicon (M_1). The network can be modified by transition metals and group III metals for enhanced hardness (M_2) or unlinked nanoparticles (np). The degree of cross-linking is adjusted by the amount of functional groups (R1, R2) which can be also linked to the substrate and the ratio of non-cross-linking organic groups without covalent bonding to the network (S).

4. Experimental

4.1. Materials Synthesis

Organic-inorganic hybrid coatings are synthesised with respect to the mechanical stability of the resulting coatings. Two main sol-gel systems are selected in order to generate basic information about the wear caused by liquid impact on these materials.
The first sol-gel system (Sol A) consists of Glycidoxypropyltrimethoxysilane (GPTMS) and Tetraethylorthosilicate (TEOS) in different mol ratios (2 : 1; 1 : 1; 1 : 2). The mixture was hydrolysed using 0.05 M HNO_3 (r_W = 1). In addition Sol A-(1 : 1) is modified using nanoparticles (ZrO_2) in the range of 10 nm (27.5 wt%).
The second sol-gel system (Sol B) is composed of Glycidoxypropyltrimethoxysilane (GPTMS), Aminopropyltriethoxysilane (APTES), Phenyltrimethoxysilane (PTMS) and Aluminium-sec-butoxide (AlB) in the ratio 6.5 : 0.4 : 1 : 2. Before mixing AlB with the silanes, Acetoacetic acid ethyl ether is added in the ratio 1:1. Hydrolysis is carried out using deionised water (r_W = 1,14). After hydrolysis is completed the system is ready to be used for the coating process. Additionally, some sol-gel systems were reinforced by nanoparticles (ZrO_2) in the range of 10 nm (30 wt%). The used particle amounts arise from the maximum particle concentration applicable during synthesis.

4.2. Coating Process

The coating solutions are applied by dip coating on aluminium samples (AA2024 clad) coated by an epoxy primer. The withdrawal speed is fixed at 0,005 m/s. After drying at room temperature for 2 h the samples are cured at 120 °C for 1 h.
Commercialised erosion protection products (PUR) are deposited on aluminium samples (coated by epoxy primer) by spraying, acting as reference. Product-A consists of a multi-layer of a flexible thick rubbery-like coating underneath a standard aircraft external top coat. Product-B is an erosion resistant rubbery-like top coat (~100 µm) on an epoxy based primer.
All samples are aged for 24 h at 60 °C before further testing.

4.3. Characterisation

All samples are characterised regarding their film thickness using the eddy current method according DIN EN ISO 2360. The adhesion of the coatings on the substrate is analysed by the cross cut test (EN ISO 2409, GT 0 = no spalling, GT 5 = complete spalling). Adhesion is measured prior to 14 days water immersion at room temperature (pre H_2O) and afterwards (post H_2O).
The flexibility is investigated by impact tests (ISO 6272) and mandrel bending tests (ISO 1519). The scratch resistance is tested according to ISO 1518. The equivalent Vickers hardness and the Young's modulus of Sol-B are measured using an Berkovich indentor. The evaluation is carried out according a modification of DIN EN ISO 14577 done by Oliver & Pharr [19].
The sample surface is investigated after the erosion test by optical microscopy.

4.4. Erosion testing

A great number of test methods are described to investigate the resistance against damage caused by liquid impact in section 2. Within this study a simple, cheap but reliable test method is applied using a high velocity water jet (Fig. 6).
Although the generated droplet size of this test method is not comparable to rain droplets (1.2 mm), the results of these tests are sufficient to distinguish between the protection properties against liquid impact of sol-gel derived coatings compared to available erosion protection coatings on the market.
The distance between the nozzle of the water jet and the sample surface is fixed at 300 mm in order to provoke the decomposition of the continuous jet into droplets at ~250 m/s (40 MPa) and ~350 m/s (70 MPa). The analysis of the droplet diameter by phase Doppler anemometry (PDA) results in droplet diameters starting from 0,3 mm down to below 0,1 mm. [14].

The water jet moves across the sample surface at two different feed speeds: 0.017 m/s and 0.25 m/s which result in exposure times of 4.8 s and 0.32 s per water jet crossing respectively. Inspection of

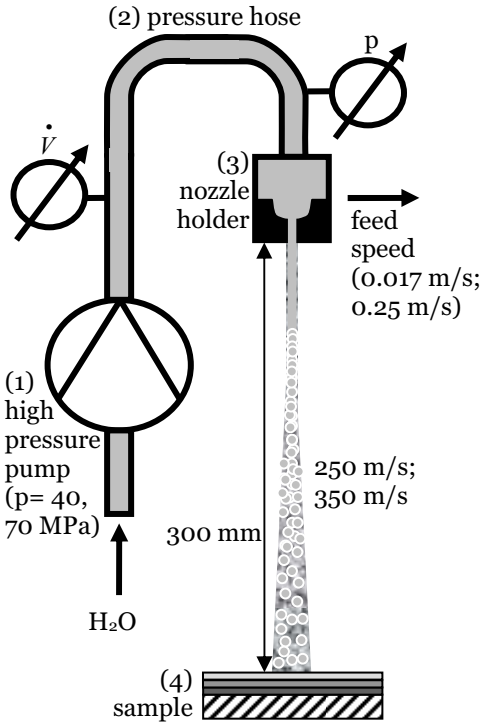

Fig. 6: Schematic drawing of the stationary sample erosion test (SSET). Water is compressed to 40 and 70 MPa by a high pressure water pump (1). A pressure hose (2) carries the water to the nozzle holder (3) which is able to move horizontal across the sample at different feed speeds. The sample (4) is placed 300 mm in distance from the nozzle to provoke the decomposition of the continuous jet into droplets.

the samples are carried out after each crossing of the water jet recording the number of crossings until (1) the first damage of the erosion protection coating is visible, (2) the substrate (primer) is visible for the first time and (3) total damage of the coating occurred (the coating is permanently eroded along the whole lane where the water jet had moved across). Thus, four different parameters were tested (Tab. 1).

Tab. 1. Key parameters for erosion testing by liquid impact using a high velocity water jet.

Pressure [MPa]	Velocity of droplets [m/s]	Feed speed [m/s]
40	250	0.017
40	250	0.25
70	350	0.017
70	350	0.25

5. Results

5.1. Layer thickness

The layer thickness of the sol-gel derived topcoats and the commercially available erosion protection products on the primer are listed in Fig. 7.

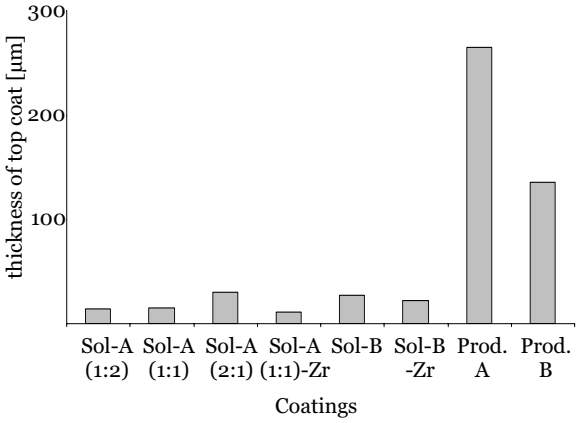

Fig. 7: Thickness of the topcoats on a 47 µm thick primer. Sol-gel derived erosion protection coatings are up to 23 times thinner than commercialised products (Sol-A-Zr: 11.4 µm; Product-A: 265 µm).

Thickness of the primer beneath all coatings is 47 µm. The sol-gel coatings are deposited between film thicknesses of 11.4 – 29.4 µm. Comparable erosion protection coatings exhibit film thicknesses between 135 – 265 µm. Thus, sol-gel derived erosion protection coatings are up to 23 times thinner than commercialised products.

5.2. Adhesion

The adhesion of the erosion protection coatings to the substrate is shown in Fig. 8.

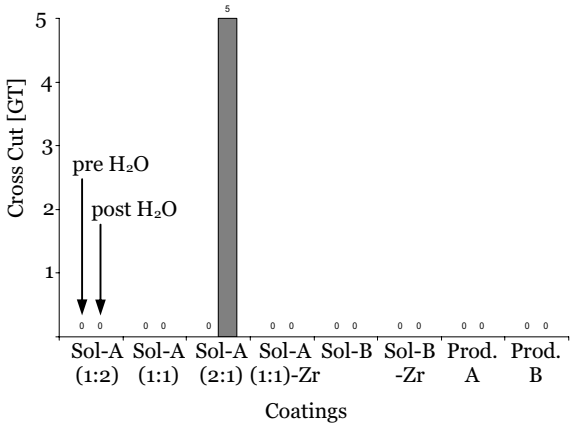

Fig. 8: Adhesion measured by cross cut test (ISO 2409, GT 0 = no spalling, GT 5 = complete spalling). The adhesion was measured prior to 14 days water immersion at RT (pre H_2O) and afterwards (post H_2O).

Good adhesion of the sol-gel derived erosion protection coatings and the available erosion protection products on the primer is detected. One sol-gel system (Sol-A-(2:1)) is not stable against water.

5.3. Flexibility

The flexibility of the samples is recorded using two test methods: The impact test and the mandrel bending test. The tests are considered as passed, when no cracks are observable and the coating sticks to the substrate without spalling.

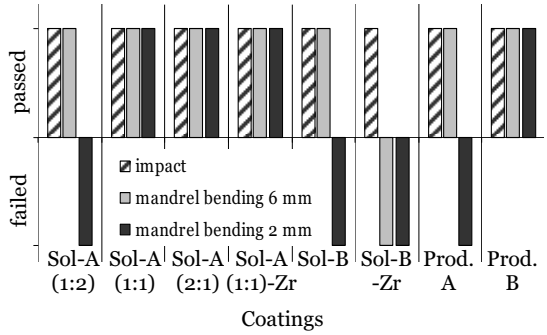

Fig. 9: Results from impact and mandrel bending tests. All samples are flexible enough to pass the impact test. Less flexible coatings failed the mandrel bending test.

Fig. 9 shows that all coatings are flexible enough to pass the impact test (hatched). Beside product-A, which tears during the 2 mm mandrel bending test due to the high layer thickness (265 µm) three sol-gel systems failed the mandrel test. Sol-A-(1:2) is synthesised using a large amount of inorganic precursor (TEOS) compared to the remaining sol-gel systems based on a related formulation. Assuming that the epoxy group of GPTMS is not cross-linked in the Sol-A system, it acts as a non-cross-linked organic spacer increasing the flexibility. Thus, less GPTMS in the system means a higher degree of cross-linking which is accompanied by less flexibility.
Sol-B exhibits harder parts derived from AlB incorporated in the coating network that may cause a reduction of flexibility (mandrel bending 2 mm failed). The reinforcement of Sol-B with a high amount of ZrO_2 nanoparticles (30 wt%) increases the hardness of the system in an additional way. Consequently, Sol-B-Zr fails the mandrel bending test using the 6 mm and the 2 mm mandrel.

5.4. Scratch resistance

The scratch resistance of the erosion protection coatings is measured according ISO 1518. Fig. 10 shows the maximum load on the sample surface applied by a steel ball of 1 mm diameter until the coating is scratched to the substrate. Commercialised erosion protection products with high layer thickness can not be scratched to the substrate up to the maximum load of 5000 g. This test method is hardly applicable for thick coatings.

Compared to the erosion protection products, where the maximum load is defined as the load which causes a continuous scratch to the substrate, the sol-gel coatings were rated by a scratch to the primer beneath. This evaluation method allows a better distinction of the scratch resistance of these coatings.

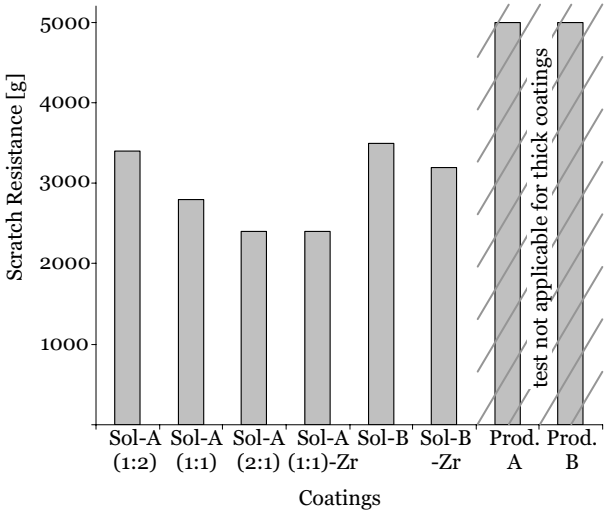

Fig. 10: Scratch resistance of the sol-gel derived erosion protection coatings and available erosion products.

Considering the variation of the GPTMS/TEOS ratio in Sol-A, it can be clearly stated that a higher degree of inorganic parts in the network (TEOS) leads to a higher scratch resistance. Contrary to expectations, the reinforcement of Sol-A-(1:1) by ZrO_2 nanoparticles results in a reduction of the scratch resistance (Sol-A-(1:1): 2800 g; Sol-A-(1:1)-Zr: 2400 g).
Sol-B exhibits hard compounds (AlB) in the sol-gel network which leads to a similar scratch resistance as Sol-A with a high inorganic content (Sol-A-(1:2)). In accordance with the nanoparticle reinforcement of Sol-A, this process also weakened the scratch resistance of the Sol-B system. Regarding the fact that common amounts required for increasing the scratch resistance are in the range of 1 wt%, it can be assumed that the used amount of nanoparticles (Sol-A: 27.5 wt%; Sol-B: 30 wt%) is too high for the purpose of improving the mechanical stability.

5.5. Hardness

The hardness and the Young's modulus of Sol-B is analysed by nanoindentation. The average values of loading-unloading curves of three different maximum loads (300 mN, 100 mN, 30 mN, dwell time: 3 s) are shown in Fig. 11. The increase of penetration depth at constant maximum load is an indicator for the creep properties of the coating material. Comparing Sol-B to erosion resistant products creeping is found to be much less. The load curves of different maximum loads are lying upon each other and the loads are applied within the same time period. Materials showing high creeping would produce different loading curves when the time for creeping is varied. This means that the elastic part of the whole deformation is high for Sol-B.

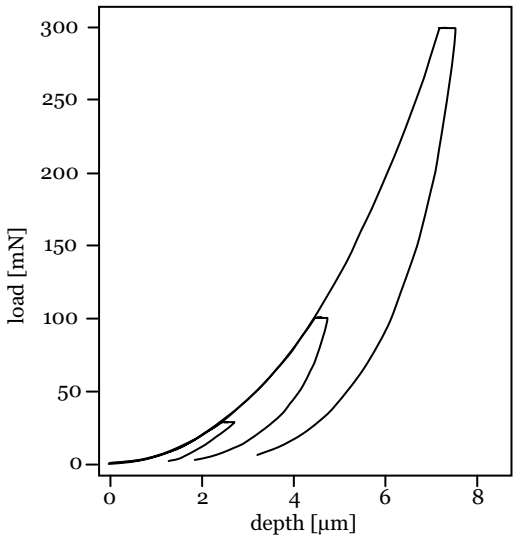

Fig. 11: Average value (10 measurements) loading-unloading curve of Sol-B at three different maximum loads (300 mN, 100 mN, 30 mN; loading: 10 s, dwell time: 3 s, release: 4 s).

Regarding the differences in penetration depths prior and after the indention visco-elastic behaviour is identified. However, there is no permanent imprint observable after the indentation even after a maximum load of 300 mN. This founding is an important evidence that these visco-elastic materials tend to heal up. No investigations are made on the time the material needed for recovering itself into the initial position.
Sol-gel coatings in general exhibit higher hardness values (Sol-B: 0.224 GPa at a penetration depth of 2.229 µm) than rubbery like erosion protection products (0.0052 GPa at a penetration depth of 4.946 µm). A rough comparison of sol-gel derived erosion protection coatings to existing erosion protection solutions with respect to the Young's modulus shows that these coatings ($E \approx 3$ GPa) feature higher stiffness than rubbery like organic coatings ($E \approx 0.01$ GPa) and are much less stiff than plasma deposited or thermal sprayed coatings ($E >> 100$ GPa).

5.6. Erosion resistance

All samples are analysed according to their rain erosion resistance using the stationary sample erosion test. The parameters used for sufficient distinction of the erosion resistance against liquid impact are a droplet velocity of 250 m/s and a feed speed of 0.017 m/s (Fig 12).

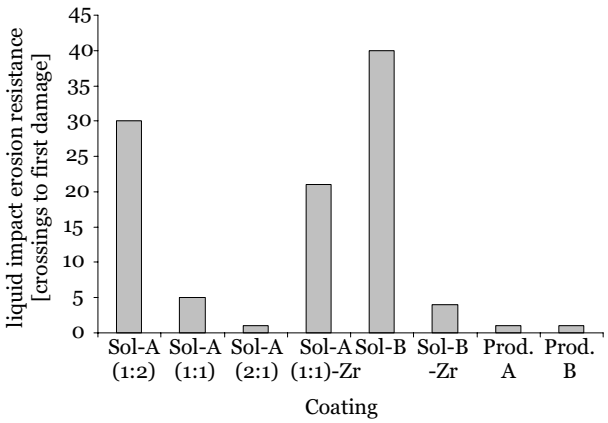

Fig. 12: Liquid impact erosion resistance of sol-gel derived coatings and available erosion protection products. The results are obtained by stationary sample erosion test at 250 m/s applying a feed speed of 0.017 m/s. High erosion resistance is reflected in a high number of crossings by water jet until first damage of the coatings occurs.

The results of the erosion tests give information about the necessary design of a sol-gel derived erosion protection coating. The variation of the ratio GPTMS/TEOS in the Sol-A network clearly shows that less GPTMS and accordingly less organic compounds leads to higher liquid erosion resistance (crossings to first damage: Sol-A-(2:1): 1; Sol-A-(1:2): 30). A higher amount of GPTMS decreases the degree of inorganic cross-linking which has a negative effect on the erosion protection performance of the coating. The nanoparticle reinforced version of Sol-A-(1:1) (Sol-A-(1:1)-Zr) exhibits increased erosion resistance (crossings to first damage Sol-A-(1:1): 5; Sol-A-(1:1)-Zr: 21). Thus, addition of nanoparticles dispersed in the sol-gel network has a positive impact on the erosion performance. However, the improvement is less than for a comparable but higher inorganic cross-linked coating (Sol-A-(1:2)) without nanoparticles. Similar to the variation of the GPTMS/TEOS ratio the higher inorganic cross-linked system exhibits increased erosion resistance.

Sol-B with its harder sol-gel particles embedded already in the sol-gel network (AlB) and a higher degree of cross-linked organic groups (GPTMS, APTES) and the tailored flexibility of the system (PTMS) shows the best erosion protection against liquid impact within this study. The high velocity water droplet load to first damage is 40 times higher compared to thick erosion protection coatings available on the market (Prod.-A, Prod.-B). The nanoparticles dispersed in the Sol-B network (Sol-B-Zr) have a negative effect on the erosion protection properties of the coating. The high organic content in the Sol-B system causes limited inorganic cross-linking between the ZrO2 nanoparticles and the inorganic part of the sol-gel matrix. Thus, the uncombined particles in the coating matrix decrease the mechanical strength of the material resulting in an earlier start of erosion damage compared to the non particle reinforced system.
Comparing Sol-A and Sol-B it seems to be promising to follow a concept as described in section 3. Evaluation of the results obtained from Sol-A would lead to the design of a high cross-linked inorganic coating. The fact that Sol-B withstands the highest number of crossings by high velocity water jet without erosion damage proves that a combination of hard compounds (AlB) in a cross-linked (GPTMS, APTES) but flexible (PTMS) inorganic-organic hybrid coating gives better protection against the erosion of the material. The aluminium-based parts in the network provide enough hardness against the high velocity droplet impact, cross-linked organic and inorganic groups avoid the crack formation due to the impact and the unlinked organic groups provide the required flexibility to absorb the impulse transferred by the water droplet.

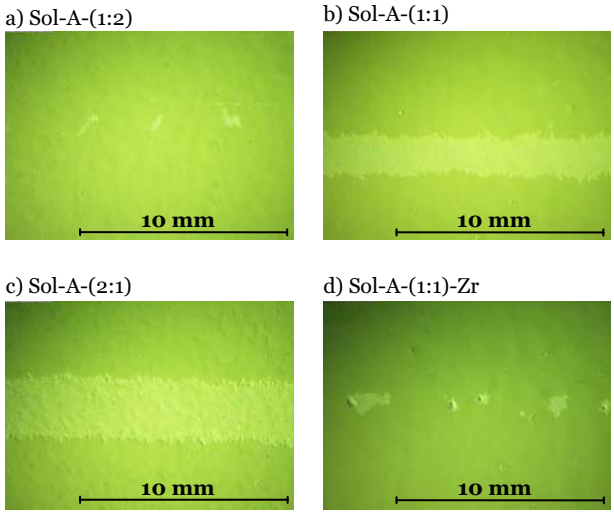

Fig. 13: Light optical microscope analysis of variations of Sol-A coated on primer. The pictures are taken after the erosion test ($v_{droplet}$ = 350 m/s, feed speed = 0.017 m/s, 1 crossing). Coatings from Sol-A-(1:1) and Sol-A-(2:1) are completely eroded to the primer at these conditions whereas Sol-A-(1:2) and Sol-A-(1:1)-Zr show only little damage.

The findings of optical inspection during the erosion test can be supported by light optical microscope analysis of the sample surface at a fixed number of crossings at constant conditions. Fig. 13 shows the sample surface of Sol-A after the erosion test at 350 m/s at a feed speed of 0.017 m/s. All pictures are taken after one water jet crossing. Coatings from Sol-A-(1:2) display only little eroded areas after the test. Sol-A-(1:1) and Sol-A-(2:1) are completely eroded to the primer whereas the erosion lane of the sol containing a higher organic content (Sol-A-(2:1)) is eroded in a

wider range than the coating deposited from a sol with less organic compounds. Comparing Fig. 13 a)-c) where the organic non-cross-linked compound is increased constantly demonstrate an increasing erosion rate with increasing amount of GPTMS.
Fig. 13 b) and Fig. 13 d) are pictures of coatings produced from the same sol-gel system but the latter is reinforced by ZrO_2 nanoparticles. Comparing the damage after similar conditions the nanoparticle reinforcement is found to be effective against liquid impact.
As can be seen already from light optical microscopy at certain high velocity water droplet loads the sol-gel derived coatings are only partly eroded showing undamaged areas in between (Fig. 13 a), d)).
This study considers the existing undamaged areas between eroded areas as a sign for cohesive failure of the coating which is explained as follows: In case of adhesive failure the coating would be completely eroded over the full length of the erosion lane.

6. Discussion

6.1. Coating matrix

The variation of precursor ratio in a simple two-component inorganic-organic hybrid system (Sol-A) gives information on the impact of the organic content and the degree of cross-linkage on the mechanical stability of a sol-gel derived system. A higher amount of organics (GPTMS) leads to a higher layer thickness of the dip coated sample which is due to the non-cross-linked organic spacer. The latter is also responsible for increased flexibility of the system (passed 2 mm mandrel bending test), but the reduced degree of cross-linking reduces the resistance to water immersion which goes back to the fact that water is able to infiltrate into the micropores of the coating and sub-surface migration may occur. This finding can be supported applying lateral forces on the sample surface resulting in little scratch resistance of the organic-rich system (Sol-A-(2:1)) compared to the inorganic-rich one. The reduced erosion resistance of the organic-rich version of Sol-A (Sol-A-(2:1)) is a consequence of the lack of cross-linking in the Si-O network due to a higher amount of non-cross-linking organic groups.
Comparing Sol-A (silica-based network, variation of amount of non-cross-linked organic spacer in the network) to Sol-B (silica-alumina-based network, cross-linked and non-cross-linked organic groups in the network) the latter follows more the idea of combining hard components and flexible properties. The hardness and the degree of cross-linking are high enough leading to failure of the 2 mm mandrel bending test. However, the produced material properties are highly efficient against liquid impact. Even the highest cross-linked version of Sol-A (Sol-A-(1:2)) indicates an earlier start of erosion damage than it is the case for coatings from Sol-B. It seems to be promising using nonsilicates in the sol-gel network (e.g. AlB) and cross-linking organic groups (APTES, GPTMS) to improve the hardness of the coating as well as non-cross-linking organic groups (PTMS) to increase the flexibility of the system. The successful combination of hard and pliant compounds within one coating material of Sol-B is also reflected considering the results from nanoindentation. Sol-B displays a high value for the Young's modulus compared to rubbery like organic commercialised erosion protection coatings. Additionally, the creeping properties of the coating material are limited due to organic cross-linking (visco-elastic properties), but the non-cross-linking organic groups in the sol-gel network allow the system to be elastic enough to recover into its initial position several hours after indentation.

6.2. Particle reinforcement

The idea of reinforcing the sol-gel network by hard inorganic particles in the nanometre scale offers different effects on the erosion resistance. It has to be considered that the used amounts of particles are relatively high (Sol-A: 27.5 wt%, Sol-B: 30 wt%) compared to common values used to improve the scratch resistance (~1 wt%).
No negative effect on the flexibility by nanoparticle reinforcement can be observed in case of Sol-A, since coatings from Sol-(1:1)-Zr pass the 2 mm mandrel bending test. The amount of non-cross-linked organic groups (GPTMS) in the Sol-A network is high enough to compensate the increased hardness by addition of nanoparticles. However, the nanoparticles in the coating matrix have a negative impact on the scratch resistance. The particles are homogeneous dispersed and particularly bonded to the inorganic part of the sol-gel network. This increase in inorganic cross-linking supports brittle material properties, which decreases the scratch resistance of the coating. Unlike scratch resistance the addition of inorganic particles influences the erosion resistance in a positive way. The particle reinforced version of Sol-A withstands up to four times higher numbers of crossings by high velocity water jet without any visible erosion damage compared to the similar formulated non particle reinforced system. The inorganic linkage between particle and matrix involving a higher degree of cross-linkage increases the resistance against liquid impact.
Sol-B shows similar effects regarding flexibility and scratch resistance. Adding high amounts of particles to Sol-B (2 mm mandrel bending test

failed) leads to further loss in flexibility (Sol-B-Zr: 2 mm and 6 mm mandrel bending test failed) and a decrease of scratch resistance due to the higher degree of inorganic cross-linking and the resulting more brittle material behaviour. Contrary Sol-A the particle reinforcement of Sol-B decreases the erosion resistance by 90 %. Sol-B is based on a completely different coating matrix exhibiting a higher organic content than the Sol-A system. Thus, inorganic cross-linking of particles and matrix is limited which causes earlier material failure after liquid impact. In addition, the reduced bonding of particles to the matrix supports particle growth which may act as surface defects that promote first cracks in the layer. Hence, it is obvious that erosion damage after high velocity rain droplet load can be observed earlier than for a comparable but homogenous built network.

7. Conclusion

The sol-gel technology offers the possibility to synthesise organic-inorganic hybrid systems which are promising materials for the use as rain erosion protection coatings.
A simple variation of a two precursor sol-gel system (TEOS/GPTMS) gives information about the necessary degree of cross-linking and the inorganic content of the polymer network for the synthesis of an erosion resistant topcoat. The investigations show that sol-gel derived coatings feature key properties required for the design of materials for enhanced erosion resistance: excellent adhesion to the substrate, flexibility, and hardness. The best results can be obtained by a combination of hard compounds and flexibility promoting groups. The hardness is adjusted by cross-linking the organic and the inorganic groups as well as reinforcing the network by hard inorganic particles. The flexibility is driven by non-cross-linked organic spacers in the sol-gel network. The coating properties are visco-elastic tending to elastic behaviour (indenter imprint disappears within 14 h).
Reinforcing the sol-gel network by nanoparticles in the range of 10 nm can have a positive effect on the erosion resistance due to the increase of the hardness. Using high amounts (30 wt%) the nanoparticles can disturb the homogeneous network formation which leads to weak erosion protection of the deposited coatings.

Reference

[1] A.A. Fyall; R.B. King, Proceedings of the Rain Erosion Conference, Royal Aircraft Establishment, Farnborough, England, May 1965

[2] A.A. Fyall; R.B. King, Proceedings of the 2nd Meersburg Conference on Rain Erosion and Allied Phenomena, Royal Aircraft Establishment, Farnborough, England, August 1967

[3] A.A. Fyall; R.B. King, Proceedings of the 3rd International Conference on Rain Erosion and Associated Phenomena, Royal Aircraft Establishment, Farnborough, England, August, 1970

[4] A.A. Fyall; R.B. King, Proceedings of the 4th International Conference on Rain Erosion and Associated Phenomena, Royal Aircraft Establishment, Farnborough, England, May, 1974

[5] J.E. Field, Proceedings of the 5th International Conference on Erosion by Liquid and Solid Impact, Royal Aircraft Establishment, Farnborough, England, September, 1979

[6] Characterization and determination of erosion resistance, ASTM, STP474, June 1969

[7] G.S. Springer, Erosion by liquid impact, Scripta Publishing, Washington, 1976

[8] BWB, Handbuch Regen-Erosion, 1979

[9] G.Y. Richards, C.S. Lei, W. Tabakoff, International Journal of Rotating Machinery 1, 9 (2003) 35-40

[10] M.J. Jackson, J.E. Field, British Ceramic Transactions 99 (2000) 1

[11] M.B. Lesser, J.E. Field, Ann. Rev. Fluid Mech. 15 (1983) 97-122

[12] C.F. Kennedy, A.R. Davies, J.E. Field, Erosion Facilities at the Cavendish Laboratory, 6th Edition, Cambridge, 2003

[13] R.J. Wasley, Stress Wave Propagation in Solides, Marcel Dekker Inc., New York NY, (1973) 87

[14] W. Milchers, Abtrag von Polymeren mit dem reinen Wasserstrahl, PhD Thesis, Hannover, 2001

[15] A.A. Deom, M. Lemistre, D.L. Balageas, Proceedings of the 18th International Congress on Instrumentation in Aerospace Simulation Facilities (1999) 29.1-29.8

[16] M.K. Lee, W.W. Kim, C.K. Rhee, W.J. Lee, Metallurgical and Materials Transactions A, 30A (1999) 961

[17] C.J. Brinker, G.W. Scherer, Sol-Gel Science, Academic Press (1989)

[18] G. Philipp, H. Schmidt, J. Non-Crystalline Solids, 82 (1986) 31-36.

[19] W. C. Oliver, G. M. Pharr, J. Mater. Res. 7 (1992) 1564-1583